Interferometer setup for detecting photon-number dependent phase shifts

Anthea Christina Nitsch

Bachelorarbeit in Physik
angefertigt im Institut für Angewandte Physik

vorgelegt der
Mathematisch-Naturwissenschaftlichen Fakultät
der
Rheinischen Friedrich-Wilhelms-Universität
Bonn

August 2023

I hereby declare that this thesis was formulated by myself and that no sources or tools other than those cited were used.

Bonn, 02.08.2023 .....
Date Signature

1. Referee: Prof. Dr. Sebastian Hofferberth
2. Referee: Prof. Dr. Simon Stellmer

Contents

CHAPTER 1

Introduction

Quantum networks provide new possibilities and challenges in science, e.g. in quantum computing, communication and meteorology. One important aspect in the development of quantum networks is the option to connect different, remote quantum systems. Such connections require carriers, which can reversibly convey quantum information. Due to their fast traveling speed and their relatively small interaction cross-sections, photons are ideal candidates to act as these carriers. Despite their small interaction range, photons can be made to interact with nonlinear media to transfer their carried information [1, 2].

In order to use photons as carriers of quantum information, controlling individual photons becomes necessary. There are multiple options to control single photons and different applications have been demonstrated [3, 4]. Controlling single photons requires nonlinear media, e.g. Rydberg atoms [5, 6, 7]. One important property of the photons that can be controlled is the phase. It has been shown in several experiments, that the phase of photons interacting with a nonlinear medium is differently influenced depending on whether one or two photons are present in a given place during a small time interval [8]. The phase shift photons experience due to a nonlinear medium is called the conditional phase shift.

The conditional phase cannot be extracted from measuring the intensity of a single laser beam since the frequency of light in the visible spectrum is on the order of a couple hundreds of THz. However, conditional phase shifts introduced by a nonlinear medium for low photon numbers can be detected with an interferometer. To reach this goal, the phase of a single photon must be distinguished from the phase of a photon when an second photon is present in a small time intervall.

At the Rubidium Rydberg Nonlinear Quantum Optics experiment in Bonn research is conducted in the area of manipulating single photons. The goal of this thesis is to build an interferometer which is capable of measuring conditional phase shifts and is able to perform under real experiment conditions. The interferometer described in this thesis is built for an implementation in an existing experiment. The development of such an interferometer in this experiment was started by Anna Speier [9]. In this thesis, based on her work the interferometer was further characterized and tested by building a test setup. This test setup has dimensions closer to the interferometer, which will later be implemented in the main experiment. For this implementation, the interferometer discussed by Tomer Zohar in her Maser thesis [8] was used as a model. In her thesis, she achieved a free-space π conditional phase for two photons as well as photon bunching due to attractive interactions in the dispersive regime.

The focus of my thesis is to test and implement the adjustments needed for introducing the interferometer in an experimental setup to measure a conditional phase shift. To give a short overview over the theoretical background, in chapter 2 a description of the classical interference of two light beams and of photon statistics in a light beam at low intensities is given. In the second part of this chapter the setup of the implemented interferometer is presented and discussed. Chapter 3 starts with a description of the method by which the interference signal can be reconstructed for low photon numbers. Building on these steps, the adjustments and characterization of the interferometer which are needed to measure a conditional phase shift in an experiment are explained. As a part of these changes, a method for optimizing the signal reconstruction is introduced and the interferometer stability is examined. The pulsed experiment sequence is implemented, being realized by implementing a sequence of time intervals in which the interference signal can be measured. Lastly, the method for measuring the conditional phase shift is discussed. It is important to note, that in this thesis no nonlinear media were introduced to create a nonlinear phase shift. In chapter 4, a short summary of this thesis is given, the results are discussed and an outlook to the necessary further steps to implement the interferometer into an experimental setup are given.

CHAPTER 2

Theory & Setup

In the first part of this section, the necessary theoretical background to understand the interference of the light in the interferometer discussed in this thesis is given. The behavior of classical and non-classical light is described based on [10] to understand the beat signal measured in the interferometer as well as the photon statistics for a low number of photons. The second part of this chapter consists of a detailed presentation of the interferometer setup used in this experiment.

2.1 Interferometry & Beat note

2.1.1 Classical interference

Classically, the form of electromagnetic waves can be derived from the Maxwell equations

$$\nabla \cdot \mathbf{D} = \rho \tag{2.1}$$

$$\nabla \cdot \mathbf{B} = 0 \tag{2.2}$$

$$\nabla \times \mathbf{E} = -\frac{\partial \mathbf{B}}{\partial t} \tag{2.3}$$

$$\nabla \times \mathbf{H} = j + \frac{\partial \mathbf{D}}{\partial t} \tag{2.4}$$

where ρ is the free charge density and j is the free current density. $\mathbf{E}$ and $\mathbf{B}$ are the electric and magnetic field. Furthermore, $\mathbf{D}$ is the electric displacement and $\mathbf{B}$ is the magnetic equivalent. They are related to the electric and magnetic field via the relations

$$\mathbf{D} = \epsilon_0 \epsilon_r \mathbf{E} \tag{2.5}$$

$$\mathbf{B} = \mu_0 \mu_r \mathbf{H} \tag{2.6}$$

When now considering the Maxwell equations in one dimension with no free charges $\rho = 0$ and currents $j = 0$, two differential equations with wave-like solutions for both fields can be written as

$$\frac{\partial \mathbf{E}_x}{\partial z} = -\frac{\partial \mathbf{B}_y}{\partial t} \tag{2.7}$$

$$-\frac{\partial \mathbf{B}_y}{\partial z} = \mu_0 \epsilon_0 \epsilon_r \frac{\partial \mathbf{E}_x}{\partial t} \tag{2.8}$$

The solutions of these differential equations have the form

$$\mathcal{E}_x(z,t) = \mathcal{E}_{x0} \cos(kz - \omega t + \Phi) \tag{2.9}$$

$$\mathcal{B}_y(z,t) = \mathcal{B}_{y0} \cos(kz - \omega t + \Phi) \tag{2.10}$$

where $\mathcal{E}_{x0}$, $\mathcal{B}_{y0}$ are the amplitudes, $k = \frac{n\omega}{c}$ is the wave vector and Φ is the optical phase. From the solution for the electric field, the intensity $\langle I \rangle$ can be calculated via

$$\langle I \rangle = \frac{1}{2} c \epsilon_0 n \mathcal{E}_x^2 \tag{2.11}$$

From the equations 2.9 and 2.10 follows, that the classical description of light of a given frequency contains two important quantities, the amplitude and the phase. In an experimental setup, the amplitude can be derived directly by measuring the intensity of the laser beam with a photo detector, whereas the phase of a light beam is determined with interferometric measurements. A simple interferometer setup is shown in figure 2.1.

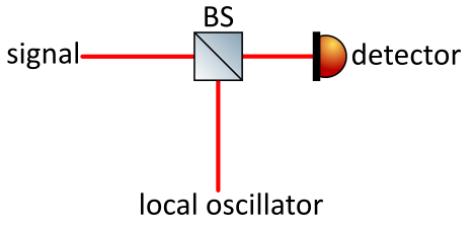

Figure 2.1: Interferometer sketch

In this setup a laser beam of interest, the signal beam, is overlapped with a reference beam called the local oscillator (LO) by a beam splitter (BS). Depending on the coherence of both beams, they interfere.

Interferometers are used for a vast variety of applications. Within optics it is common to distinguish between two different types. The homodyne and the heterodyne interferometer, depending on the frequencies of the signal beam and the local oscillator beam. In the case where the local oscillator and the signal beam have the same frequency, it is called homodyne. In case of different frequencies, the interferometer is called heterodyne [10]. In this thesis, the interferometer is heterodyne as will be discussed in the following sections.

The intensity $\langle I \rangle$ of an interference of two electromagnetic waves of arbitrary amplitudes and different

frequencies is described by

$$\langle I \rangle \propto \left(E_{Sig} \cos\left(\omega_{Sig} t\right) + E_{LO} \cos\left(\omega_{LO} t\right)\right)^2 \tag{2.12}$$

$$= E_{Sig}^2 \cos^2\left(\omega_{Sig} t\right) + E_{LO}^2 \cos^2\left(\omega_{LO} t\right) + 2E_{Sig}E_{LO} \cos(\omega_{Sig} t) \cos(\omega_{LO} t) \tag{2.13}$$

where ω_{Sig} and ω_{LO} are the angular frequencies and E_{Sig} and E_{LO} are the amplitudes of the signal beam and the local oscillator respectively. With the trigonometric identities

$$\cos A \cos B = \frac{1}{2}\cos(A - B) + \frac{1}{2}\cos(A - B) \tag{2.14}$$

$$\cos^2 A = \frac{1}{2}(\cos(2A) + 1) \tag{2.15}$$

the intensity of the interference signal becomes proportional to

$$\begin{aligned}\langle I \rangle \propto \frac{E_{Sig}^2 + E_{LO}^2}{2} + \frac{1}{2}(E_{Sig}^2 \cos(2\omega_{Sig} t) + E_{LO}^2 \cos(2\omega_{LO} t)) \\ + E_{Sig}E_{LO}(\cos((\omega_{Sig} - \omega_{LO})t) + \cos((\omega_{Sig} + \omega_{LO})t))\end{aligned} \tag{2.16}$$

Equation 2.16 holds for arbitrary frequencies. For the experimental setup discussed in this thesis, the frequencies of the local oscillator and the signal beam are large and of the same order. For light near the visible spectrum the frequencies are on the order of hundreds of THz. Within this limit the relation

$$\omega_{LO}, \omega_{Sig} \gg \left|\omega_{Sig} - \omega_{LO}\right| \tag{2.17}$$

is valid. This leads to the averaging out of the terms with fast oscillations over time. Therefore, only the part of equation 2.16 with no dependency of ω and the part including the difference of the two frequencies remain. Furthermore, a phase shift $\Delta\varphi$ between the signal and the local oscillator beam can be introduced, leading to the additional term in equation 2.18. The intensity of the interference signal can then be described as

$$\langle I \rangle \propto \frac{E_{Sig}^2 + E_{LO}^2}{2} + E_{Sig}E_{LO} \cos((\omega_{Sig} - \omega_{LO})t + \Delta\varphi) \tag{2.18}$$

Relation 2.18 consists of two parts. A constant offset stemming from the time-averaged fast-oscillating frequency components and an oscillating signal, whose oscillation frequency depends on the difference of the frequencies of the signal ω_{Sig} and the local oscillator ω_{LO}. This interference signal can be measured classically with the interferometer. It is called the beat signal. The additional phase shift $\Delta\varphi$ in the argument of the oscillation will later be relevant, when recreating the beat signal from the raw data. In case the two frequencies in equation 2.18 are identical, the resulting intensity can be modulated by changing their phase difference. For different frequencies of the local oscillator and the signal beam, the intensity will oscillate over time. Equation 2.18 can be used later to generate a probability distribution for photons in a simulation of the expected beat signal. In this simulation the beat signal is examined for different strengths of E_{Sig} and E_{LO}.

2.1.2 Photon statistics

Where classically a perfectly coherent light beam consists of an electromagnetic wave, in quantum theory it can be described as a stream of photons. This description of a light beam later becomes relevant, because in the interferometer setup implemented in this thesis we are interested in working with a low photon rate, where the classical description is no longer completely applicable and has to be expanded. The following content is based on [10].

When considering a perfectly monochromatic beam with the angular frequency ω and constant intensity I, the photon flux Φ can be defined as

$$\Phi = \frac{IA}{\hbar\omega} \tag{2.19}$$

where A is the cross section area of the beam.

Contrary to the classical expectations of no intensity fluctuations and therefore no photon flux changes over time there must be statistical fluctuations on short time-scales due to the discrete nature of the photons.

In a light beam of constant intensity, the average number of photons $\overline{n}$ in a longitudinal beam segment of the length L is given by

$$\overline{n} = \frac{\Phi L}{c} \tag{2.20}$$

where c is the speed of light. Furthermore, the probability $\mathcal{P}(n)$ of finding n segments containing one photon in a given beam with a total number of N segments and $N - n$ segments containing no photons is given by a binomial distribution

$$\mathcal{P}(n) = \frac{N!}{n!(N-n)!} p^n (1-p)^{N-n} \tag{2.21}$$

where $p = \frac{\overline{n}}{N}$. By taking the limit $N \to \infty$ of this distribution, the result is the Poisson distribution

$$\mathcal{P}(n) = \frac{\overline{n}^n}{n!} e^{-\overline{n}}, n = 0, 1, 2, \ldots \tag{2.22}$$

Therefore, the photon statistics for a coherent light source with constant intensity is given by a Poisson distribution. In a simulation of the interference of two low power laser beams this distribution describes the fluctuations of the measured photon number around the calculated average. These statistics in combination with the classical beat signal described in the preivous section 2.1.1 will later be used to generate the data for the simulation of the beat signal reconstructed from generated photon counts.

2.2 Interferometer setup

The classical interference of two laser beams and a basic interferometer setup (see figure 2.1) was discussed in section 2.1.1. The heterodyne approach is used in this thesis, following the idea implemented at the Weizmann Institute of Science [8]. With the built interferometer setup the phase of the interference signal of two laser beams can be extracted.

The basic setup is illustated in figure 2.2. The interference signal is created by splitting a laser beam into two beams with beam splitter (BS) 1 and shifting the frequency of each beam with acousto-optic modulators (AOM) separately by a different value. Even though the signal and local oscillator beam come from the same laser source this is a heterodyne detection scheme since the interfering frequencies are different. The two beams are called the local oscillator and the signal beam respectively. In figure 2.1 the laser beam passing through the atom cloud is the signal beam and the other beam is the local oscillator beam. In the final implementation, which is beyond the scope of this thesis, the signal beam will pass through some phase modifying medium, e.g. an atom cloud, after the frequency shift is applied. After that, the signal beam is split in two parts by BS 2. One part of the beam is detected by detector 2 for the measurement of the conditional phase shift. The signal measured by detector 2 is called the reference signal and is independent of the local oscillator beam. The second part of the split beam is overlapped via BS 3 and the interference signal is detected on detector 1.

AOM are used to induce the frequency shift of both beams. They consist of a crystal material, whose refractive index changes due to an oscillating mechanical strain in form of a sound wave induced by piezo elements. On this traveling strain, the light beam is partially diffracted and doppler shifted. The frequencies of the laser beams in the first diffracted order are shifted by the frequency of the sound wave in the AOM. The first diffracted order is used to create the interference signal [11].

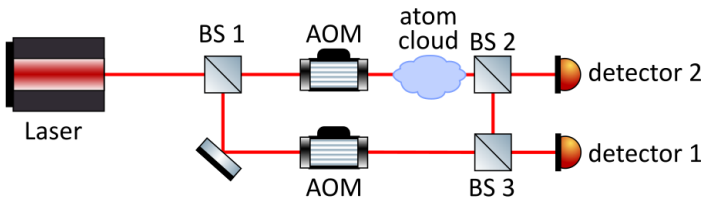

Figure 2.2: Basic interferometer setup

As an objective of this thesis, the interferometer setup is adjusted to be implemented into the Rubidium Rydberg Nonlinear Quantum Optics experiment to measure conditional phase shifts. Therefore, the following boundary condition applies. The distance, the signal beam traverses in free space, was expanded to accommodate for the additional distances in the main experiment and the conditional phase has to be measured. A sketch and photos of the implemented experimental setup are depicted in the figures 2.3 and 2.4.

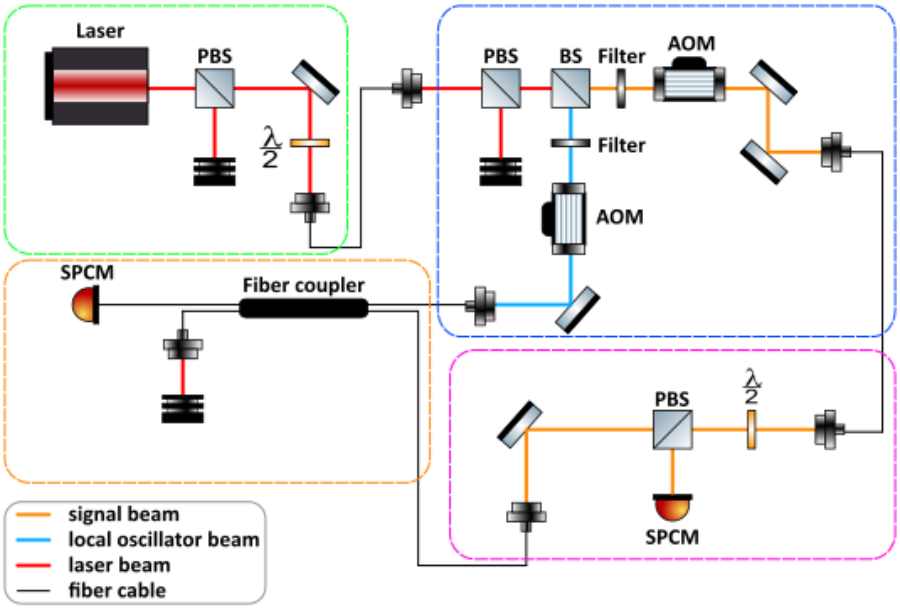

Figure 2.3: Sketch of the experiment setup

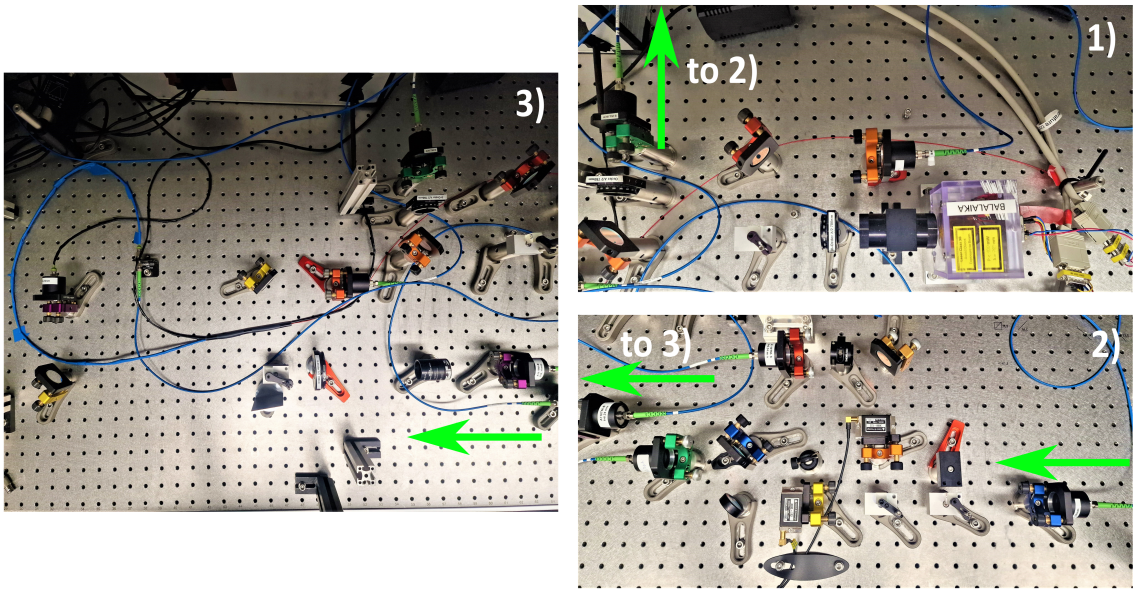

Figure 2.4: Picture of the implemented interferometer; photo 1) corresponds to the green box, photo 2) corresponds to the blue box and photo 3) corresponds to the pink and yellow boxes in the sketch of the interferometer in figure 2.3

In figure 2.3, four boxes outlined in different colors are marking different sections of the experiment setup.

In the green box the laser beam is coupled into a optical fiber after going through a polarized beam splitter (PBS) and a $\frac{\lambda}{2}$-plate. Both devices are used to ensure that the laser beam has the same linear polarization as the optical fiber. In the experiment two different lasers were used as a beam source, a self built 780 nm distributed feedback (DFB) diode laser and a extended cavity diode laser[1] (ECDL) with the same wavelength. These two lasers are subject to discussion with regard to their different phase stability in chapter 3.4.

In the blue box, the beam passes another PBS and is then split by a BS. The frequencies of the two resulting beams are then shifted by two AOM[2] by different radio frequencies. The radio frequencies used for the frequency shift by the AOM are 80 MHz and 82 MHz resulting in a beat signal with a frequency of 2 MHz and a corresponding 500 ns period. As driver for the AOM a direct digital synthesis board[3] (DDS board) is used. These radio frequencies can be generated with an accuracy on the order of 10^{-2}Hz, which leads to a slight frequency shift of the resulting beat signal. The vertical beam path in the blue box is the local oscillator beam of the interferometer and the horizontal beam path is the signal arm. The local oscillator beam is directly coupled into the fiber coupler. The intensity of the beams in both interferometer arms is reduced by introducing neutral density filters into the setup. The reduction of the intensity of the laser beam has the goal to reduce its photon rate such that it can be measured in terms of single photons.

The light in the signal arm is coupled into an additional optical fiber and in the pink box the laser beam is split again. One part of the beam is led to a single photon counting module[4] (SPCM), the other part of the beam is coupled into the fiber coupler. SPCMs are used to measure signals at low intensity levels. They create voltage pulses for incoming photons. Due to the dead time of the SPCMs, no more than 1 million photon counts per second can be registered without taking the dead time of the SPCM into account and calculating the resulting correction factor. This is why the light intensity is modulated to stay below that value. Atoms or other media inducing a phase shift could be introduced to the setup behind the PBS in the signal arm.

In the yellow box, the signals from the local oscillator arm and the signal arm are brought to interference inside the fiber coupler. This polarization maintaining fiber coupler[5] has a 99:1 ratio of the output signals. The 99 % signal is then detected by a SPCM. The other signal is led into a beam dump. By using a fiber coupler instead of a BS the interference of the two beams can be achieved in a more reliable and stable way. Both SPCMs in the setup are connected to a time tagger[6], which collects and saves the measured data. In this experiment the **FileWriter** saving method was used [12]. With this method the time tagger records the time of the rising flanks of the signals on its channels as a time-tag stream. For e.g the measurement of the times of the incident photons, this means that the rising flanks of the voltage peaks created by the SPCMs are recorded.

[1] VitaWave ECDL-7830R
[2] Gooch & Housego AOMO 3080-122
[3] Analog Devices EVAL-AD9958
[4] Laser Components' Count
[5] Thorlabs PN780R1A2
[6] Swabian Instruments TimeTagger 20

CHAPTER 3

Interferometer characterization

In this chapter the data processing as well as the adjustments needed to insert the interferometer into an experiment setup to measure the phase shift are discussed. This discussion builds on the theory and setup introduced in chapter 2. To measure the conditional phase in an actual experiment several characteristics of the interferometer should be considered and examined. Those characteristics are

- the method for retrieving the beat signal from single detected photons
- the reliable extraction of a period with which the beat signal can be reconstructed,
- an optimal ratio of local oscillator and signal beam strength,
- a sufficiently large time over which the period is stable, in order to prevent external phase shifts from having a too big influence on the phase and
- that the conditional phase shift works with the experiment conditions.

3.1 Data treatment

As discussed in section 2.2, the detected signal consists of a low rate of incident photons. The intensity is reduced to such an extend that the classical description is not completely accurate anymore and the laser beam has to be treated like a flow of single photons.

In a measurement of raw data, meaning the voltage peaks created by incident photons detected by the SPCMs, the mean count rate of the detected photons is always chosen to be smaller than 1 MHz. The mean count rate is defined as the number of photons detected by the SPCM per second. This choice of the upper limit of the mean count rate is made due to the dead time of the SPCM (see section 2.2). The mean count rate translates to an average of 0.5 photons detected per a 500 ns period of the beat signal. The period of the beat signal results from its frequency of 2 MHz. The number of detected photons per period fluctuates between different measurements since the conditions surrounding the interferometer can change.

In figure 3.1, such a measurement of the photons of the interference signal detected by an SPCM is depicted. The mean count rate in the depicted measurement is 712 kHz resulting in an average of 0.36

photons detected per period of the beat signal. This is not sufficient to recreate the beat signal. This is illustrated in figure 3.1 by the single photon detection events shown as vertical blue lines and the extracted classical beat signal (the method used to extract the beat signal is discussed in the following) indicated as a dashed gray line.

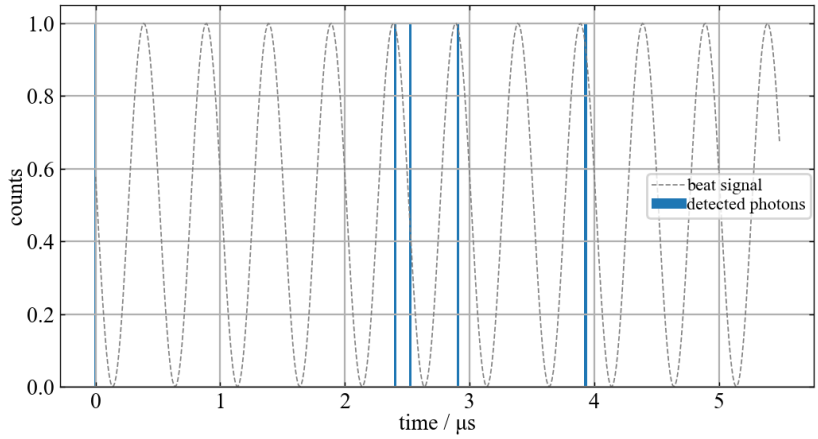

Figure 3.1: Raw photon data saved with **FileWriter**

From the figure it becomes apparent that the beat signal cannot be directly extracted from the raw data, which makes some post-processing necessary. In order to recover the beat signal, the detected photons are summed up over many full periods of the beat signal to restore a single period of the beat signal, where the oscillation is visible. This means, that photon detection times modulo the period of the beat signal is calculated and entered into a histogram. In the following this process is called folding of the data.

The resulting histograms for different numbers of detected photons are shown in figure 3.2. While in figure 3.2(a) the beat signal is barely discernible for a photon number of 100, by folding the beat signal so that 1000 photons contribute to the histogram as shown in figure 3.2(b) the shape of the beat signal is recognizable to some extent. For larger numbers of folded photons the beat signal can be reconstructed more accurate (see figures 3.2(c) and 3.2(d)).

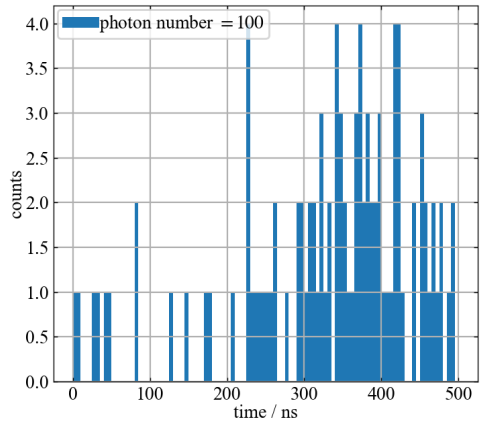

(a) Beat signal recreated with 100 photons

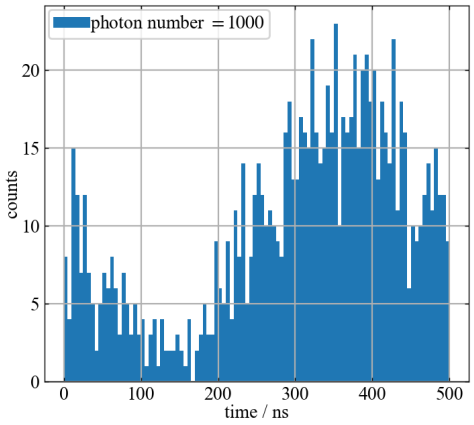

(b) Beat signal recreated with 1 000 photons

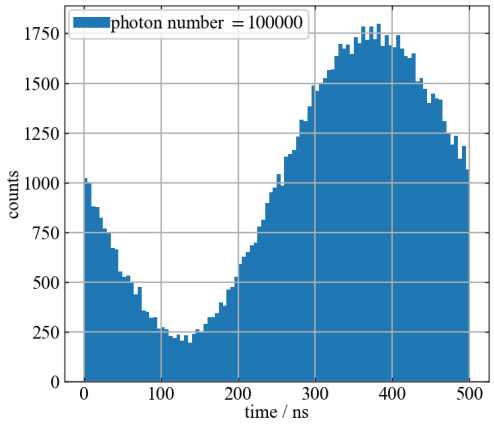

(c) Beat signal recreated with 100 000 photons

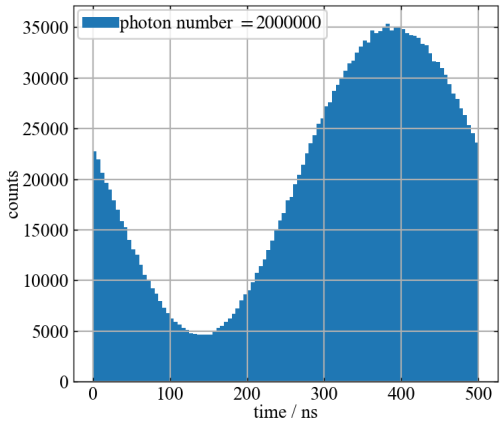

(d) Beat signal recreated with 2 000 000 photons

Figure 3.2: Beat signal recreated with different numbers of photons

The folding of the data gives an indication of how many photons have to be measured to extract the beat signal. By fitting a function of the form given in equation 2.18 to the data, the phase can be extracted. For lower numbers of photons, the uncertainty on the extracted phase increases. This happens, because there is not enough data to accurately describe the beat signal. With more detected photons, the phase can be more accurately described pending external influences leading to a phase shift. This will be discussed in more detail in section 3.4.

3.2 Trigger signal

As explained in section 2.2, the beat signal does not have an exact frequency of 2 MHz but varies slightly. Because of this inaccuracy, the period of the measured beat signal deviates slightly from the exact period of the beat signal, which one would get if the frequency shifts generated by the AOM were exact. If the data is folded over many periods of 500 ns, but the real period of the beat signal is a little bit larger or

smaller, the oscillation corresponding to the folding period and the actual beat signal will run out of phase. Since the period of the beat signal of500 ns is small compared to the measured time scales of several seconds, a small deviation of the period with which the raw data is folded in figure 3.2 from the accurate period has a big impact on the extracted beat signal. For an inaccurate period the summed up intervals experience a phase shift compared to each other. This is shown in figure 3.3.

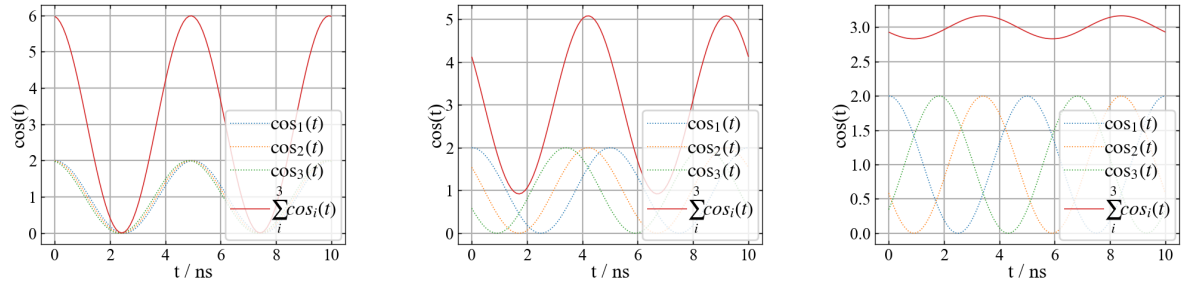

(a) Oscillations shifted by $\varphi = 0.1$ rad (b) Oscillations shifted by $\varphi = 1$ rad (c) Oscillations shifted by $\varphi = 2$ rad

Figure 3.3: Illustration of phase shift induced by a wrong folding period

In this figure three oscillations (thin blue, green and orange lines) are added up to a resulting signal (red line) for different phase shifts. For slight phase shifts (see figure 3.3(a)), the oscillation consisting of the three added up oscillations is clearly recognizable and has a large amplitude. For stronger phase shifts in the figures 3.3(b) and 3.3(c) the amplitude decreases drastically and the phase of the resulting oscillation is shifted.

If the beat signal is folded with a folding period that deviates significantly from the actual period of the beat signal, the beat signal will not be visible in the folded signal. Therefore, to reliably determine the folding period without having to guess it, a trigger signal is implemented.

The trigger signal is created with the frequency output of the DDS board separately from the beat signal created in the interferometer. To generate this signal the 80 and 82 MHz signals from the DDS board (which are also connected to the AOMs) are split up and amplified. The amplified signals are then combined on a phase detector[1]. The output of the phase detector is an oscillating signal which contains both the sum and the difference of the 80 MHz and 82 MHz frequencies in accordance with equation 2.18. The high frequencies are filtered out with a low-pass filter. The resulting beat signal is converted to a box signal via a comparator[2] circuit to ensure, that the slope of rising flanks is steep enough to get a sharp peak on the time tagger. The time tagger can record the times of the rising flank of the box signal which are used as the trigger signals. The difference of two consecutive time stamps can be used as the folding period.

The trigger signal is shown in figure 3.4. It can be folded similarly to the beat signal in figure 3.2 with the difference that, instead of the rising flanks of the voltage pulses created by the SPCM for detected photons, the recorded times of the rising flanks of the box signal are folded. With this the time distribution of the trigger signal can be shown. This plot gives an indication on how large the jitter in

[1] Mini Circiuts ZRPD-1+
[2] Analog Devices LT1715

time of the trigger signals is. In figure 3.4(a) the time between two consecutive trigger signals is shown to be on the order of the period of the beat signal. The exact value of the folding period in the considered measurement is $T = 500.0720922\,\text{ns}$. Furthermore, in figure 3.4(b) the time distribution of the trigger event folded with the mean period in between consecutive events is depicted.

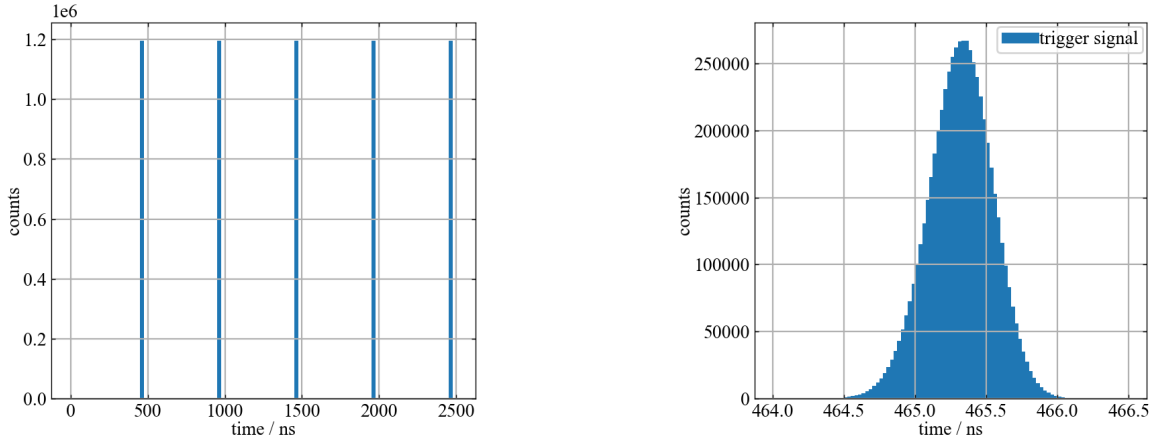

(a) Folding trigger signal

(b) Trigger signal folded with the folding period between two consecutive signals

Figure 3.4: Folding trigger signal detected by the time tagger recorded with the **FileWriter** method

By using the trigger the measured data can now be folded over the correct period without having to determine the folding period by trial and error. The folding period is extracted from the trigger signal by taking the mean over the time in between each rising flank of the box signal generated from the beat signal. Time differences which deviate too much (more than 2 ns) from the theoretical period are filtered out. Shorter time intervals between consecutive signals could result from the time tagger measuring two events on one rising flank of the box signal. This could occur, if the threshold above which the time tagger records an event is crossed twice due to noise on the signal. Time intervals which are too long can be caused by the same effect leading to a small delay of the recorded trigger signal. A tight bound around the predicted period gives the most reproducible results.

In figure 3.5, the reconstructed beat signal is plotted for different folding periods illustrating the problem of a folding period deviating by a percentage from the actual period of the beat signal extracted from the trigger signal. The beat signal shown in figure 3.5(d) is determined by using the period extracted from the trigger signal. The other three figures 3.5(a), 3.5(b) and 3.5(c) are folded with periods that are longer than the one extracted from the trigger signal. Qualitatively, it can be seen, that the folded signal depends strongly on the deviation of the folding periods. While the phase and amplitude of the beat signal vary in figure 3.5(b) and 3.5(c) compared to the beat signal reconstructed using the folding period extracted from the trigger signal in figure 3.5(d), in figure 3.5(a) the beat signal is not discernible.

To examine the impact of the different folding periods on the beat signal, the phase, contrast and the time, after which the folding period extracted from the trigger signal and the deviating folding periods are completely out of phase, are discussed in the following.

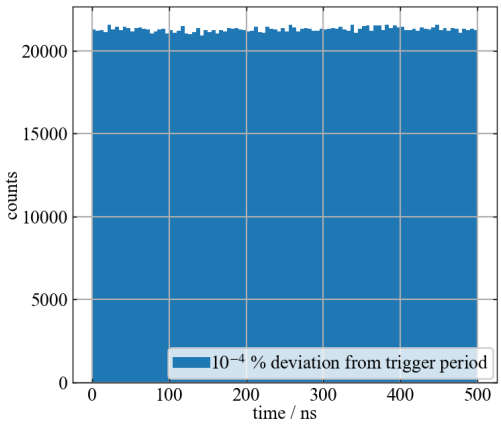

(a) Folding period T deviating by 10^{-4}%: T = 500.0725923 ns

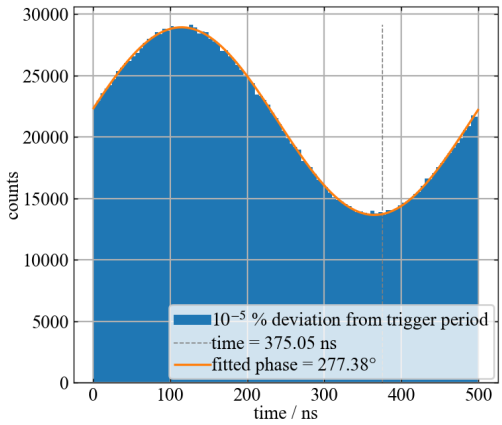

(b) Folding period T deviating by 10^{-5}%: T = 500.0721422 ns; contrast: $C = (0.3588 \pm 0.0012)$

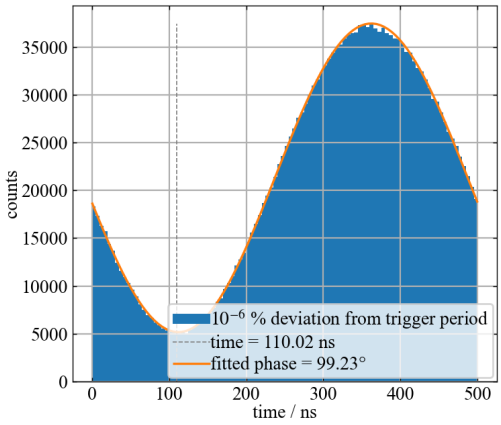

(c) Folding period T deviating by 10^{-6}%: T = 500.0720972 ns; contrast: $(C = (0.7573 \pm 0.0021)$

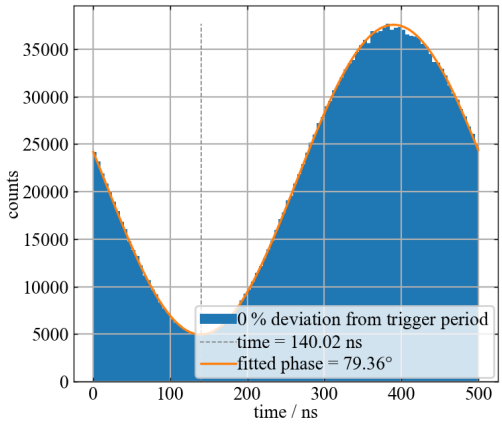

(d) Folding period T extracted from trigger signal T = 500.0720922 ns; contrast: $C = (0.7670 \pm 0.0018)$

Figure 3.5: Beat signal for different folding periods deviating slightly from the folding period extracted from trigger signal. The data was taken over a time of 3 s and a number of 1 921 145 photons was summed up

The phase of the folded signal can be determined by fitting a function $f(t)$ of the same shape as described in equation 2.18 to the recreated beat signal.

$$f(t) = a \cdot \cos\left(2\pi \cdot \frac{1}{\text{folding period}} \cdot t + \varphi\right) + b \tag{3.1}$$

The fitted function is indicated as an orange line in figure 3.5. The determined phases for the different deviations are listed in table 3.1.

The phase of $(79.36 \pm 0.14)^\circ$ extracted from the fit to the folded signal with the trigger period as folding

period is the phase relative to the trigger signal. This relative phase is determined by the length of cables and the optical path and it is expected to have some drifts over time. The magnitude of these drifts will be considered later in this chapter. Therefore, a stable phase φ is not to be expected and its value varies with time.

deviation / %	phase φ / °
10^{-4}	-
10^{-5}	277.38 ± 0.19
10^{-6}	99.23 ± 0.15
0	79.36 ± 0.14

Table 3.1: Fitted phases for different deviations from the folding period extracted from the trigger signal

It can be seen, that even for a small percentage deviation from the folding period extracted from the trigger signal, the phase varies strongly. For a 10^{-5}% or 10^{-6}% deviation the phase is shifted and for a 10^{-4}% deviation cannot be determined. Without a trigger signal it is therefore impossible to distinguish whether a phase drift comes from the interferometer itself or errors in the estimated period time for the folding process.

Another indicator of how close the folding period is to the exact folding period for the measurement is the contrast defined as

$$C = \frac{N_{max} - N_{min}}{N_{max} + N_{min}} \tag{3.2}$$

where N_{max} and N_{min} are the maximal and minimal photon numbers in the histogram of the beat signal. A contrast close to 1 means that the amplitude is large compared to the offset. This value varies for different relative powers of the local oscillator and signal beam. Therefore, only the relative change of the contrast is considered. However, the contrast is maximal for the correct folding period for the beat signal, because for deviating folding periods the phases of the consecutive periods are shifted and lead to a lowering of the contrast. In figure 3.5 it can be seen, that the contrast C is approaching but not reaching 1 when the folding period gets closer to the folding period extracted from the trigger signal. The contrasts in figure 3.5 are listed in table 3.2, where the errors in the contrast values are resulting from the fitted parameters.

deviation / %	contrast
10^{-4}	-
10^{-5}	0.3588 ± 0.0012
10^{-6}	0.7573 ± 0.0021
0	0.7670 ± 0.0018

Table 3.2: Fitted phases for different deviations from the folding period extracted from the trigger signal

As was mentioned before, the deviating folding periods lead to a phase shift of consecutive intervals. To show how fast the oscillation (see equation 2.9) with a deviating folding period gains a phase shift of π compared to the oscillation with a folding period extracted from the trigger signal, the difference of the angular frequencies calculated from both folding periods is considered. The time t it takes for both

oscillations with the frequencies f_{dev} and f_{trig} to gain a phase shift of π is described by the following equation.

$$2\pi f_{\text{dev}} t_\pi - 2\pi f_{\text{trig}} t_\pi = \pi \tag{3.3}$$

$$\Leftrightarrow t_\pi = \frac{\pi}{2(f_{\text{dev}} - f_{\text{trig}})} \tag{3.4}$$

This is an indicator for how fast the deviating folding period lead to a phase shift of consecutive single periods eventually causing the beat signal not to be recognizable. The resulting time periods t_π are listed in table 3.3.

deviation / %	t_π / s
10^{-4}	0.25
10^{-5}	2.50
10^{-6}	25.00

Table 3.3: Times at which the phase shift of the compared oscillations is π for different deviations from T_0

In addition to the deviation of the period of the beat signal compared to the theoretically determined period of 500 ns caused by the limited accuracy of the DDS board, there are time dependent shifts of the beat signal period from other external sources. One prominent example for such a time dependent shift of the period length is the frequency shift of the 80 MHz and the 82 MHz resulting from turning on the DDS board and the amplifiers. This does not only influence the beat signal but also the trigger signal generated from the same source. This means that the extracted folding periods, as the mean over trigger periods, are dependent on time and should be recalculated between measurements.

To illustrate this, the difference between the calculated period of 500 ns and the measured effective period of the trigger signal for approximately an hour after turning the DDS board on is plotted in figure 3.6.

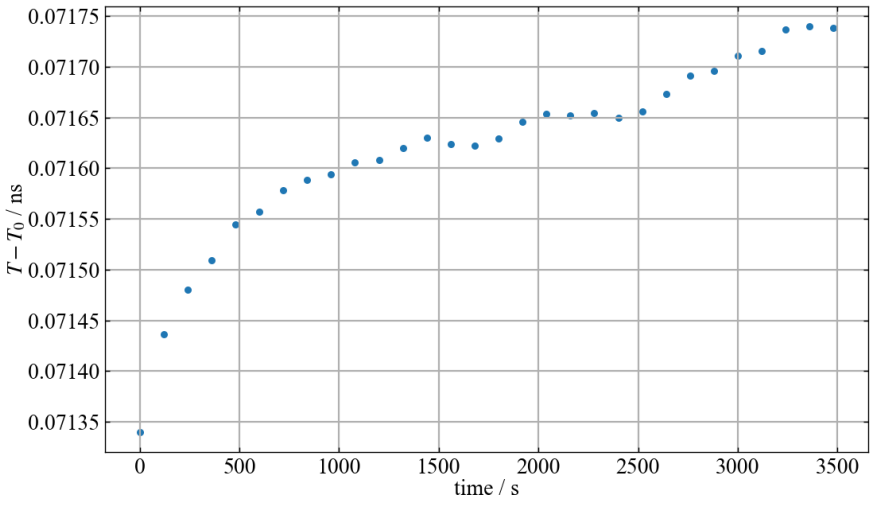

Figure 3.6: Difference between the period $T_0 = 500$ ns of the 2 MHz signal and the measured period T over time

In the first hour the period grows over time. After that, the changes in the period decrease but are still there. The frequency change in the beginning of the measurement could be caused by the warm up of the quartz crystal on the DDS board resulting in a shift of the two interfering frequencies. A fixed folding period determined directly after turning on the DDS board will give a minimal or no contrast after a couple of minutes due to this shift of the period. Furthermore, the frequency of the beat signal in the setup changes over time even after the warm up phase of the DDS board.

3.3 Simulation

In the previous sections, the method for the extraction of the beat signal from the raw photon data was described. In these theses sections, the local oscillator beam and the signal beam had a similar intensity. In other publications the local oscillator beam is often chosen to be of a higher intensity than the signal beam (see [8]). Therefore, the question arises if there is an advantage in changing the ratio of the intensities of the interfering beams. With the results from the sections 2.1.1 and 2.1.2, the expected distribution of the photons in the beat signal for low intensities can be simulated with a python program.

For this simulation, equation 2.18 is used to generate the average photon number and equation 2.22 is used to describe the fluctuation around this average value. By using the classical description with added fluctuations caused by the discrete nature of light at low photon numbers, the raw data shown in figure 3.1 can be simulated. Similarly to how the experiment data is treated (see section 3.1) the beat signal can be also be recreated from simulated raw data. In this simulation the detection efficiency of the SPCM as well as noise sources and phase drifts are not taken into account.

Using this simulation it is possible to determine, if there is an advantage to having a local oscillator which is of stronger or of equal power compared to the power of the signal in the signal arm of the interferometer. A stronger local oscillator would result in a higher photon number per time interval and a lower contrast C (see equation 3.2) of the beat signal, whereas a weaker local oscillator would lead to a higher contrast C of the beat signal and a lower photon number (see equation 2.18).

In this section, the eventual advantage of various local oscillator strengths is determined by the accuracy of the fitted phase to the generated data. Because the data is generated by a simulation, the period of the beat signal can be accurately determined. Therefore, the accuracy of the fitted phase to the generated data can be compared to the set phase φ of the generated oscillation.

In this simulation, the set phase φ is chosen to be 0. By fitting the function given in equation 3.1 with the folding period $T = 500\,\text{ns}$ to the simulated data, the accuracy of the fitted phase for various strengths of the signal beam can be examined. Due to the fact, that the period of the beat signal in this simulation can be chosen to be exactly 500 ns, the frequency of the fitting function in equation 3.1 can be fixed to 2 MHz.

The fitting of the function shown in equation 3.1 to the generated data as well as the generated folded data are shown in figure 3.7 for different ratios of the amplitudes of the local oscillator E_{LO} and the signal E_{Sig}. In this figure, 1000 periods of generated data were folded similarly to processing the real experiment data. In figure 3.7(a), the reconstructed beat signal and the fitted function are depicted for different ratios of E_{Sig} to E_{LO}. In figure 3.7(b), the beat signal and the fitted function are plotted normalized. Similarly to the beat signal constructed from experimental data, in the figures 3.7 the

generated (normalized) counts are plotted versus the time of a beat signal period. In these figures, the lower contrast C (see equation 3.2) of the oscillations for higher values of E_{LO} is visualized. As discussed in the previous section, a lower contrast indicates a lower amplitude to offset ratio of the oscillation.

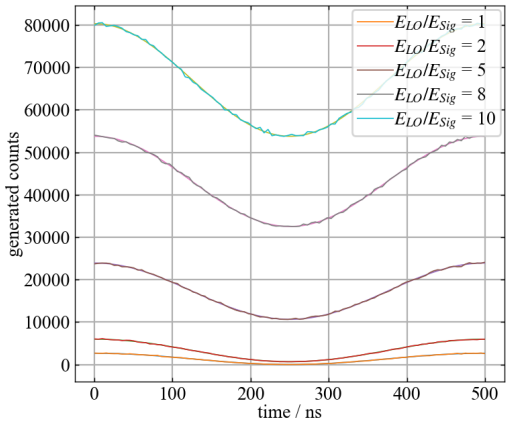

(a) Generated folded data with fitted function

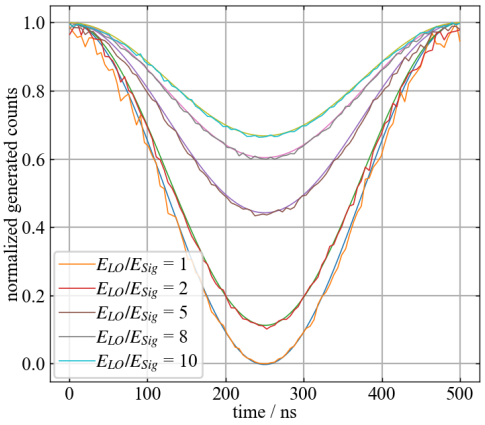

(b) Normalized generated folded data with fitted function

Figure 3.7: Simulation for different ratios of E_{Sig} and E_{LO} for 1000 folded periods of $T = 500\,\text{ns}$

It can be seen that the resulting beat signal varies in offset and amplitude with changing ratios of the amplitudes. The larger the ratio of E_{LO} to E_{Sig} gets, the larger the offset of the beat signal becomes. For ratios near 1 the offset becomes smaller. The higher offset results from more local oscillator photons being detected due to the higher intensity of the local oscillator beam for small powers of the signal beam in a given time interval. This has also the effect of lowering the contrast C of the beat signal. A lower offset leads to the opposite results.

With this simulation, the phase φ can be determined for different ratios of E_{sig} and E_{LO} and the convergence of the absolute values of the determined phases to 0° can be compared. The convergence of the determined phases φ to the value 0° plotted versus the signal strength E_{Sig}^2 of the signal beam can be seen in figure 3.8. In this figure, the logarithmic absolute value of the phase φ is plotted against the logarithm of the signal strength E_{Sig}^2.

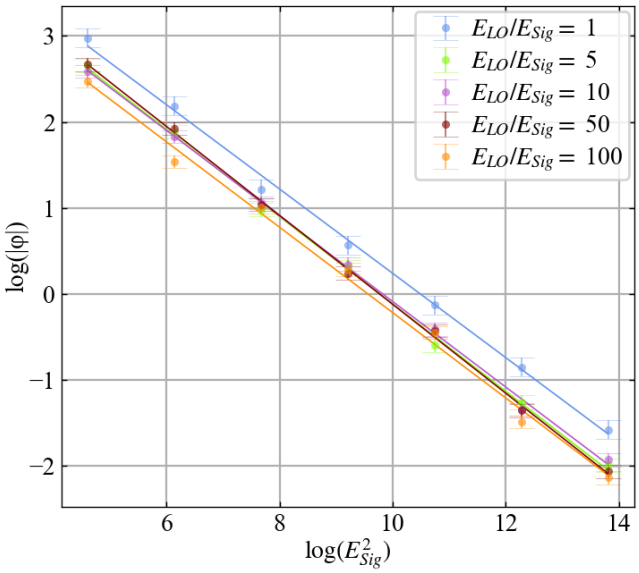

Figure 3.8: Fitted phases for variable E_{Sig}^2

To examine the slope of the curve of the fitted phases, the function

$$\varphi = \varphi_0 \cdot E_{Sig}^{2 \cdot a} \tag{3.5}$$

where a and φ_0 are the fit parameters, is fitted to the data. E_{Sig}^2 is comparable to an intensity or the number of photons. In the double logarithmic scale this function takes the form

$$\ln(\varphi) = \ln(\varphi_0) + 2a \cdot \ln(E_{Sig}) \tag{3.6}$$

To give a qualitative statement for which ratio of $\frac{E_{LO}}{E_{Sig}}$ the interfering laser beams gives the fastest conversion to the given phase, the fit parameters of the fitted linear curves are listed in table 3.4.

E_{LO}/E_{Sig}	fitted slope	fitted y intercept
1	-0.490 ± 0.012	5.14 ± 0.11
5	-0.507 ± 0.009	4.96 ± 0.09
10	-0.497 ± 0.008	4.88 ± 0.08
50	-0.517 ± 0.007	5.05 ± 0.07
100	-0.496 ± 0.016	4.74 ± 0.15

Table 3.4: Slopes a and y intercepts $\ln(\varphi_0)$ of the linear function 3.6 fitted to the fitted phases

The simulated data is created by drawing the simulated photon counts from a Poisson distribution and folding over a limited number of samples, resulting in slightly different slopes of the linear fit leading to variations of the values of the fitted slope. As can be seen in table 3.4, the fitted slopes fluctuate around the value 0.5. If the absolute value of the slope is larger, the phase φ converges faster to 0. It can be

seen, that the slopes have a similar value considering their errors. This means that the power of the local oscillator beam compared to the signal power is not crucial to get a faster conversion of the phase. The y intercept of the linear fitted functions for a ratio of the beam strengths of 1 is higher than the y intercept for the other ratios in figure 3.8. This means that, though the scaling of the fitted functions is the same, the fit gives more reliable data for a larger local oscillator strength.

The similar slopes for different ratios give evidence that the conversion of the phase does not depend on the ratio $\frac{E_{LO}}{E_{Sig}}$. Additionally, the value of the slope gives an indication, what limits the accuracy of the fitted phase for low photon numbers. As is shown in 3.4, the fitted slopes are all approximately $a \approx 0.5$. In the non-logarithmic fit function 3.5 this slope corresponds to the square root of E_{Sig}. This exponent can be understood as shot noise, which occurs due to the discrete nature of photons. This signal-to-noise ratio (SNR) scales with $\sqrt{N}$, where $N \propto E_{Sig}$ is the number of photons to which the function 3.1 is fitted [13]. This match of the fitted slope a and the scaling of the SNR is an indication that accurately determining the phase in this simulation is limited by the shot noise.

For implementing this interferometer to measure a conditional phase shift, this means that the ratio of the intensities of both interferometer arms theoretically do not have to be particularly considered for the conversion of the phases. But due to the higher y intercept for a ratio of $\frac{E_{LO}}{E_{Sig}} = 1$ the fitted phase is less accurate at a fixed strength of E_{Sig}^2. This means, that even though the fitted phase converges equally for all simulated strengths of the local oscillator, a higher uncertainty of the phase is introduced for ratios close to one. The optimal local oscillator strength cannot be deduced directly from this simulation and has to be extracted under real experiment conditions. This test under real experiment conditions is particularly important, since noise and other factors leading to a deviation of the simulated data are not taken into account in this simulation. Especially, the detection efficiency and dark counts were not considered in this simulation.

3.4 Interferometer stability

In the previous section, the simulation showed that the precision of the fitted phase improves with longer measurements in figure 3.8. In reality this is only true on timescales shorter than the interferometer drifts due to external influences. In this chapter, the Allan deviation is used to make a quantitative statement about the interferometer stability and the timescale where the phase can be estimated with the highest precision. To determine the phase stability of the interferometer in the time domain as a function of the averaging time τ the Allan variance is calculated. The Allan deviation, as the square root of the Allan variance, is a popular method for identifying and quantifying different noise terms, that can occur in oscillators and clocks [8, 14].

The Allan variance is a special case of the M-sample variance.

$$\sigma_y^2(M,T,\tau) = \frac{1}{M-1}\left(\sum_{i=0}^{M-1}\overline{y}_i^2 - \left(\frac{1}{M}\sum_{i=0}^{M-1}\overline{y}_i\right)^2\right) \tag{3.7}$$

with the sample rate M, the averaged phase or frequency $\overline{y}_i$ over the time interval $[T, T+\tau]$. For the Allan variance the sample rate is $M = 2$ which leads to

$$\sigma_y^2(\tau) = \langle \sigma_y^2(2, \tau, \tau) \rangle = \langle (\overline{y}_{i+1} - \overline{y}_i)^2 \rangle \tag{3.8}$$

Similarly to the variance, the Allan deviation is defined as

$$\sigma_y(\tau) = \sqrt{\sigma_y^2(\tau)} \tag{3.9}$$

In the following, the phase stability of the interferometer is calculated and the averaged phase will be called $\overline{\varphi}$.

In figure 3.9, the method of how to calculate the Allan deviation is illustrated. To calculate the Allan deviation, the mean phase $\overline{\varphi}$ over a time interval τ is calculated by fitting the function 3.1 to the data. A time interval of the length of the average time τ consists of the time over which the photons are folded to create one period of the beat signal in figure 3.9(b). The average time τ is an integer multiple of the beat signal period. The extraction of the phase is done by folding the detected photons (marked by colored bars in figure 3.9(a)) over the average time τ. In figure 3.9(b), the single photon counts for three consecutive time intervals $\tau_{i,i+1,i+2}$ (blue, pink and green) were folded. The folded data is shown as the blue, pink and green histograms in the lower graph 3.9(b) and the fitted functions are marked by the lines of the same color. This sketch is not entirely realistic, since the photon number varies between both plots, but serves for a better visualization of the method to determine the Allan deviation. To calculate the Allan variance, every two consecutive phases $\overline{\varphi}_i$ and $\overline{\varphi}_{i+1}$ are subtracted from each other. In figure 3.9, this would mean that $\overline{\varphi}_{i+1}$ is subtracted from $\overline{\varphi}_i$ and $\overline{\varphi}_{i+2}$ is subtracted from $\overline{\varphi}_{i+1}$. To get the Allan deviation, the mean and the square root of these differences is taken. This process is repeated for different averaging times τ.

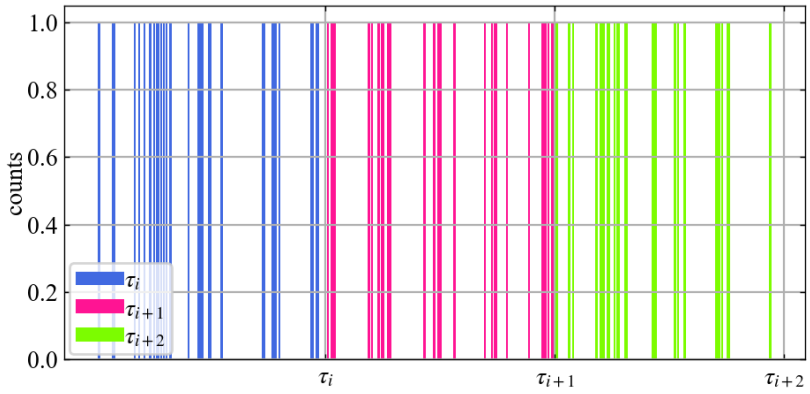

(a) Sketch of times of photon detection in consecutive time intervals of the duration τ

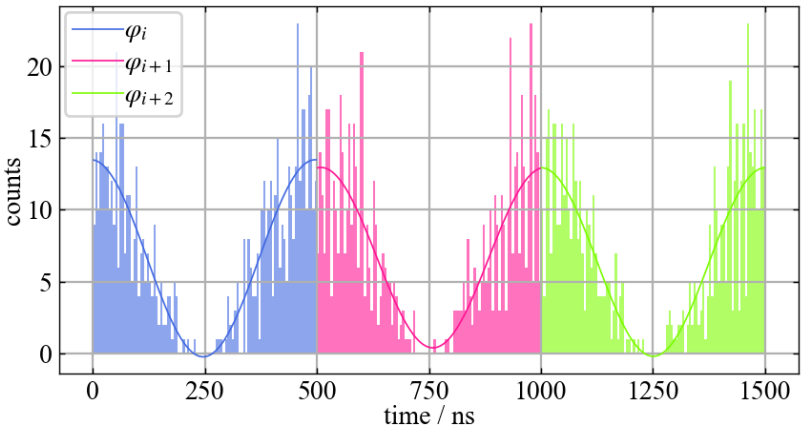

(b) Sketch of fit to the folded detected photon times with the folding interval τ

Figure 3.9: Illustration of Allan deviation

The Allan deviation for the phase of the interferometer as a function of the averaging time τ is calculated and plotted in the log-log-scale in figure 3.10. For small averaging times τ on the order of one or few periods of the beat signal, the reliable determination of the phase is limited due to the low photon number detected by the SPCM. This effect is called shot noise (see section 3.3). As discussed in section 2.2, in this interferometer setup the mean photon count rate is limited to 10^6Hz due to the dead time of the SPCM. This is no hard limit but the dead time means that nonlinear effects start to play a role on this scale. This means that on average 0.5 photons are detected within one period of 500 ns, which for low numbers of folded periods does not suffice to recreate the beat signal and extract a reliable phase.

If the averaging time τ is much larger (on the order of hundreds of milliseconds and longer) than the period of the beat signal, the extracted phase shifts due to external influences. Those influences could be an air flow or acoustic noise influencing the laser beam or the distance, the laser beam traverses in each interferometer arm. Furthermore, the glass fibers built into the experiment could expand or contract over time due to temperature fluctuations, which also leads to a phase shift of the interference signal.

These effects cannot be eliminated by the folding period extracted from the trigger signal due to the fact that the extracted period and the period of the beat signal run out of phase. The external influences leading to a phase shift of the beat signal are the limiting factor of the time over which the phase is stable.

The low photon numbers for small average times τ and the phase shifts induced by external influences for large average times τ lead to the shape of the data points plotted with blue dots in figure 3.10. First the phase stability increases (the deviation decreases) because more photons are detected until a certain average time τ_{bias} is reached at which the deviation on the phase is minimal. This point is called the **bias stability**. Then the deviation of the phase increases again due to external sources inducing a phase shift. The data points in blue in figure 3.10 were calculated with interferometer data taken with the distributed feedback (DFB) laser and shows the expected shape of the Allan deviation. The Allan deviation of the DFB laser shows that the phase is most stable over averages over about 0.016 s time intervals with a deviation of about 1°.

The beat signal was also measured with an extended cavity diode laser (ECDL) as beam source, which leads to an Allan deviation that differs significantly from the one calculated for the DFB laser. The data points for the ECDL are plotted with orange dots in figure 3.10. The orange plotted data points have a local maximum at about 3.6 ms and 14.7 ms, which are caused by correlated noise inside the laser. This means that at certain average times τ the phase is more unstable than suggested by shot noise alone.

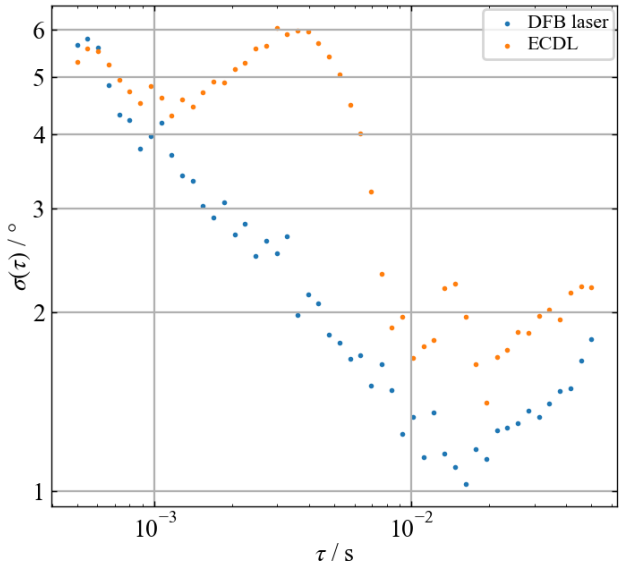

Figure 3.10: Allan deviation of the fitted phase over various time intervals for both lasers used in the experiment

The difference of the Allan deviation plots of both lasers can be caused by their different configurations.

The two types of lasers differ in how the laser cavity is formed. The resonator of the ECDL consists of the rear high-reflective facet of the laser diode and the Littrow diffraction grating. The diffraction grating acts as a wavelength selective element in this external resonator [15]. Therefore, an explanation for the peaks on the Allan deviation plot for the ECDL may be that due to mechanical vibrations of the

diffraction grating there could be instabilities in the wavelength of the laser. These instabilities could cause a higher deviation at selected averaging times τ.

The self-built DFB laser does not have such an external cavity. The whole laser resonator consists of a periodic structure, meaning that it is built with an integrated grating structure in which the light is Bragg reflected [16]. Since there are no components which could vibrate as strongly as the components of the ECDL there are no pronounced peaks in the Allan deviation plot of this laser.

To further analyze the correlated noise causing the maxima in the Allan deviation of the ECDL, the fitted phases are studied closer. In figure 3.11 the phases for the ECDL and the DFB laser are depicted over a time interval of 0.25 s. In the figure, the mean value of the phase was subtracted to better see the strength of the fluctuation of the phase.

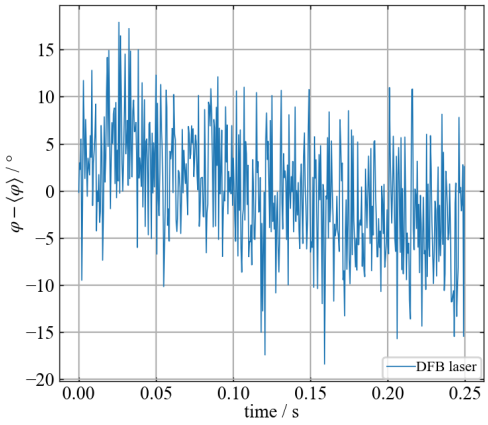

(a) Fitted phases for consecutive averaging times τ for the DFB laser

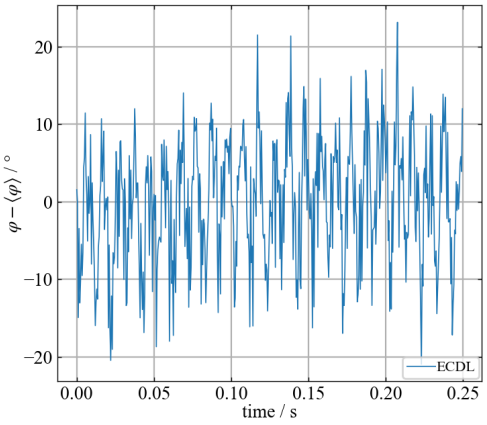

(b) Fitted phases for consecutive averaging times τ for the ECDL

Figure 3.11: Fitted phases for consecutive time intervals $\tau = 0.5$ ms; individual data points as well as errors are not plotted here to better visualize the oscillation

In figure 3.11(b), the phase curve is depicted for the ECDL. One can see, that the fitted phase oscillates. The fitted phase of the DFB laser shows the expected noise on the phase which is not periodic or time-dependent (see 3.11(a)). The maximum of the bigger peak in the Allan deviation of the ECDL is at approximately the averaging time $\tau_{max} = 3.6$ ms, which translates to a frequency of 280 Hz. By fitting a cosine function to the oscillation of the fitted phase of the ECDL (see figure 3.12) its frequency can be determined to (99.93 ± 1.18)Hz.

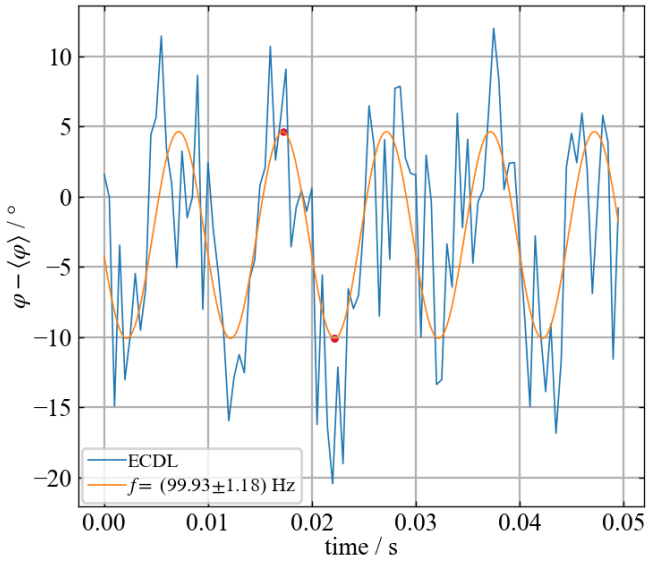

Figure 3.12: Cosine function fitted to the fitted phases for consecutive averaging times τ; to better visualize the oscillation, the error bars were not plotted

This deviates by more that a factor of two from the frequency extracted from the Allan deviation plot. But the Allan variance describes the strength of deviations of phases averaged over consecutive intervals. For a maximal deviation, the phase of consecutive intervals τ_i and τ_{i+1} would have to be situated at the minimum and the maximum of the oscillation of the fitted phase for the ECDL. This is shown in figure 3.12 by the two red dots. Therefore, the actual frequency of the additional oscillation is half the value extracted from the Allan deviation. For the oscillation extracted from the Allan deviation this gives frequency of approximately 140 Hz. The frequency extracted from the average time τ in figure 3.10 is approximately a third larger than the frequency of the oscillation in figure 3.12. The deviation can be explained by the slightly shifted maximum of the noise peak of the ECDL in the Allan deviation in figure 3.10. This shift of the maximum could result from the shot noise, which is responsible for the linear decline in the first half of the figure 3.10.

The noise leading to the larger local maximum can be illustrated. The noise causing the maximum at 14.7 ms has a frequency of approximately 30 Hz. Also, the maximum and therefore the amplitude of the oscillation is way less pronounced. The oscillation leading to this peak is not visible when plotted.

In this section, the phase stability of the interferometer in the time domain was calculated. In addition to the expected Allan deviation for the DFB laser correlated noise was discovered for the ECDL. This correlated noise could partly be visualized and explained. This means that with the Allan deviation phase noise of the ECDL could be calculated.

The Allan deviation calculated in this section makes it possible to find the time where a phase can be extracted with the highest precision, the bias stability point. From the graph 3.10, this point can be found at $(0.016\,\mathrm{s}, 1^\circ)$. However, for longer measurements the uncertainty found with the Allan deviation is only on the order of few degrees. This is why it is still possible in figure 3.2(d) to see a clear oscillation

after even 2 million folded periods translating to a time of 1 s.

3.5 Pulsed experiments

The main setup of the Rubidium Rydberg Quantum Optics experiment in the Nonlinear Quantum Optics group forces some constraints on the length of the interferometer. Further, the interferometer will probe the nonlinear medium as shown in figure 2.1. In the main experiment the nonlinear medium is a gas consisting of ultracold atoms. Since this gas needs some preparation time between measurements, the interferometer will in reality only be used in bursts. Therefore, the interferometer will be operated in a pulsed way. The interferometer performance during pulsing must be demonstrated.

To mimic this pulsed experiment sequence, the AOMs are periodically turned on and off. The light is only measured, when the AOMs deflect light into the first order (Bragg diffraction), which is coupled into optical fibers (see figure 2.3) and further used to create the beat signal.

For the pulsing of the signal a field programmable gate array (FPGA) based pulse generator is used [17]. This pulse generator is also used in the main experiment. The whole pulse generator consists of a FPGA[3] and a break out board which are connected via a board-to-board-connector. Both components are shown in figure 3.13. The FPGA is programmable and the breakout board distributes the generated signals to a number of electrical SMA outputs.

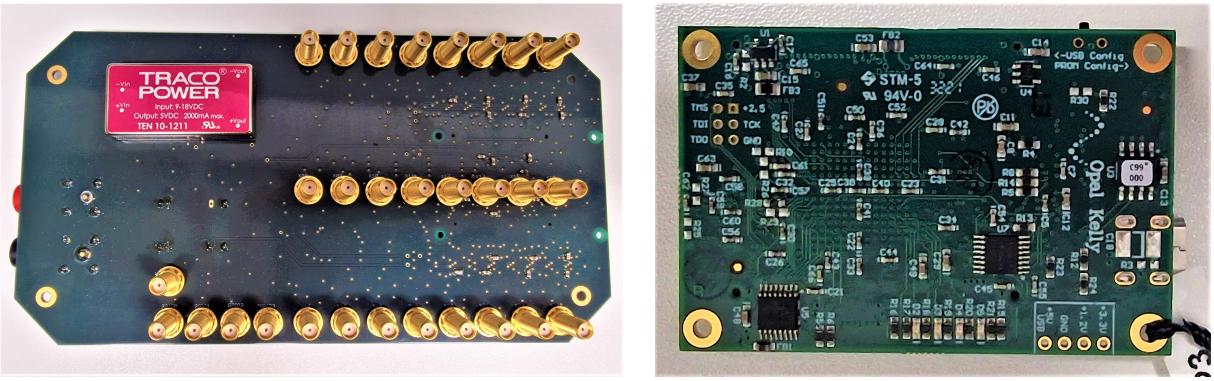

(a) Break out board (b) FPGA

Figure 3.13: FPGA based pulse generator

[3] Opal Kelly XEM3005

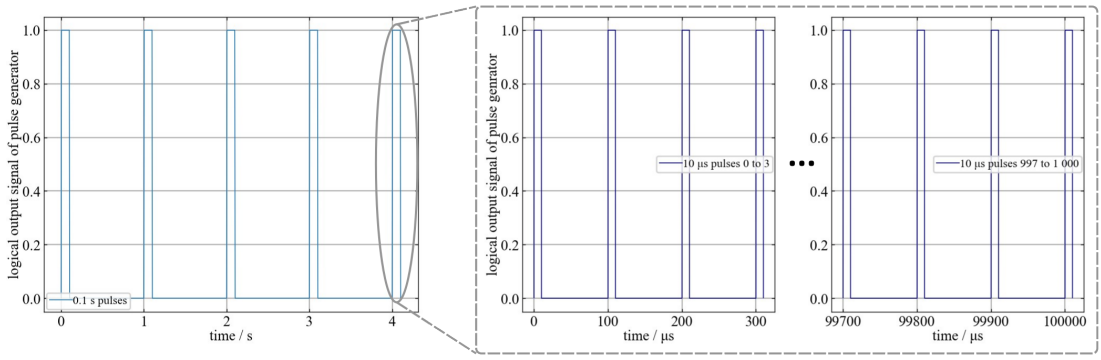

(a) 0.1 s on 0.9 s off sequence with 1000 pulses in the on time with 10 µs on and 90 µs off

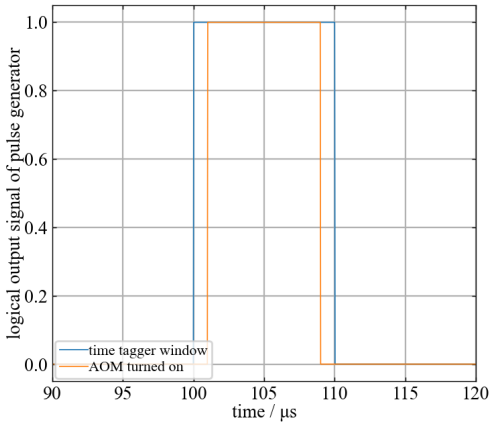

(b) Time tagger signal enveloping the signal turning the AOMs on and off

Figure 3.14: Experiment pulse sequence

The pulse generator can set different output channels to either logical 1 or 0 and so create the measurement pulse pattern. The experiment sequence in this group consists of a long preparation time and then a burst of 1000 pulses, a small break and 1000 reference pulses. Each pulse has a duration of 10 µs and there is a 90 µs downtime between consecutive pulses [18]. Two channels are used for implementing the pulses in the experiment. One serves as a TTL signal for the time tagger, indicating the pulses. The other channel is used as a TTL for the AOM radio frequency switches. In the preparation time the interferometer AOMs are switched off, and they are then turned on for a 8 µs window during each pulse using the AOM TTL channel.

The mimicked experiment sequence used for the test setup of the interferometer has a similar pattern. The main difference is that the first burst of 1000 pulses is not followed by a second burst of 1000 reference pulses. Instead, after the burst of 1000 pulses taking a time of 0.1 s, the AOMs are turned off for a time interval of 0.9 s. The pulse pattern implemented in the test setup of the interferometer is depicted in figure 3.14(a). The pulse turning the AOMs on and off is enveloped by the pulse sent to the time tagger. The time tagger window is chosen to envelope the time the AOM is turned on to mimic the

experiment conditions better and in case the form of this window varies. The signal turning the AOMs on is delayed by 1 µs compared to the signal defining the start of the time tagger window and is turned on for 8 µs. This is shown in figure 3.14(b). During the on-time of the time tagger the detected photons are further evaluated later.

With this pulse pattern, the number of detected photons is reduced due to the fact, that the laser does not continually hit the SPCM. This means that there are less photons to recreate the beat signal as well as continuous large time intervals during which the interfering laser beams are not detected. When comparing a signal, which is only measured in periodically occurring time intervals and a signal, which can be constantly measured, the shot noise in the first case is higher.

The 0.1 s and 1 µs pulse forms can be retrieved similarly to the beat signal by using the time intervals between two rising flanks recorded by the time tagger of the 0.1 s pulses and of the 1000 pulses inside several 0.1 s pulses as folding period. With these folding periods of approximately 1 s for the 0.1 s pulse and 100 µs for the pulses enveloped by the 0.1 s pulse the pulse shapes can be retrieved. The resulting pulse shapes are depicted in figure 3.15.

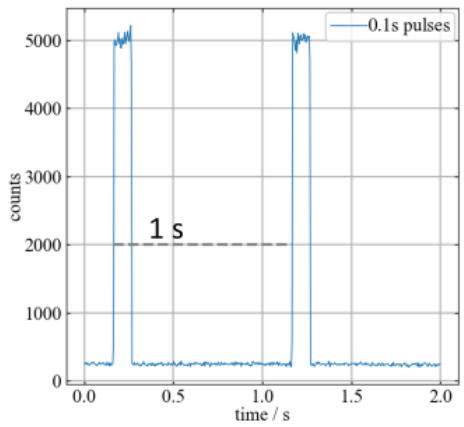

(a) 0.1 s pulses retrieved by folding the data

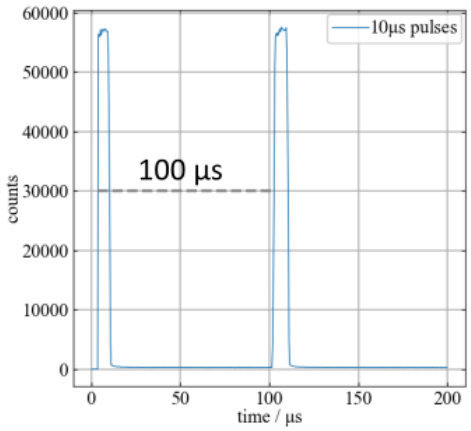

(b) 10 µs pulse inside the 0.1 s pulse retrieved by folding the data

Figure 3.15: Retrieving measured pulse shape by folding 361 263 photons over 1 s and 2 397 873 photons over 100 µs

In figure 3.15(a), two measurement pulses, each enveloping 1000 smaller pulses, are depicted. Furthermore, two of the 1000 pulses enveloped by the measurement pulse are plotted in figure 3.15(b). The small fluctuations on the signal are, similarly to the fluctuations on the beat signal in section 3.1, a consequence of folding the data.

For each measurement window, the beat signal can be retrieved in a histogram as shown in section 3.1. These histograms can be plotted together as a heat map to visualize the phase shift over time. In this heat map, the color of the fields corresponds to the number of photons measured. With this the stability of the signal over time can be shown. The resulting plots are depicted in figure 3.16.

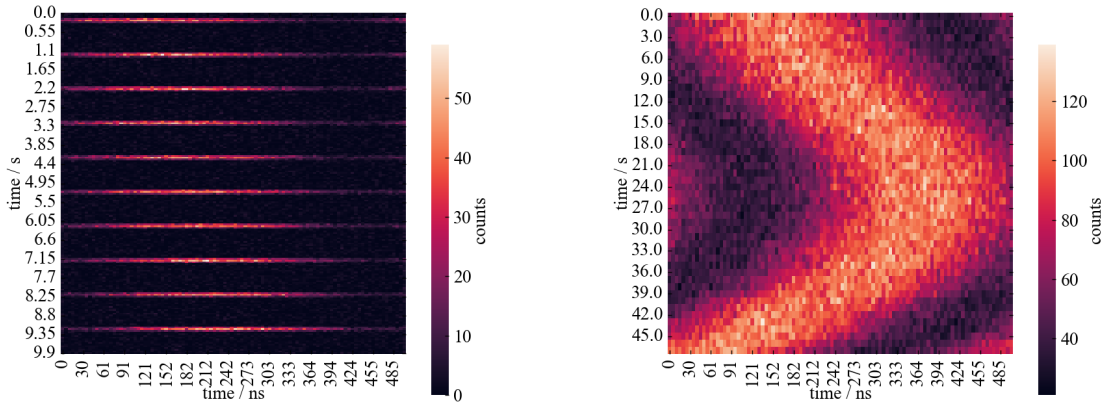

(a) Beat signal over time including the time in between measurement pulses

(b) Beat signal over 45 s with the photons measured inside the measurement pulse; the 0.9 s intervals are removed; averaged over 1000 pulses

Figure 3.16: Heat maps showing the phase drift over time inside the measurement pulses

The 0.1 s pulses can be reconstructed and the ratio of 1:9 on and off time is visualized in figure 3.16(a). Compared to figure 3.16(b) a smaller time interval is plotted. The 1000 pulses inside the measurement pulse cannot be resolved, due to the fact that the photon count inside a single pulse of 10 µs is too low. In figure 3.16(b), the phase drift over 45 s is shown. The drifting of the phase over the course of a minute is to be expected, since the bias stability time of the Allan deviation is 16 ms for the DFB laser. As discussed in section 3.4, over this time period the phase between two averaging intervals τ is most constant with a deviation of about 1°. The phase over this time period is shown in figure 3.17.

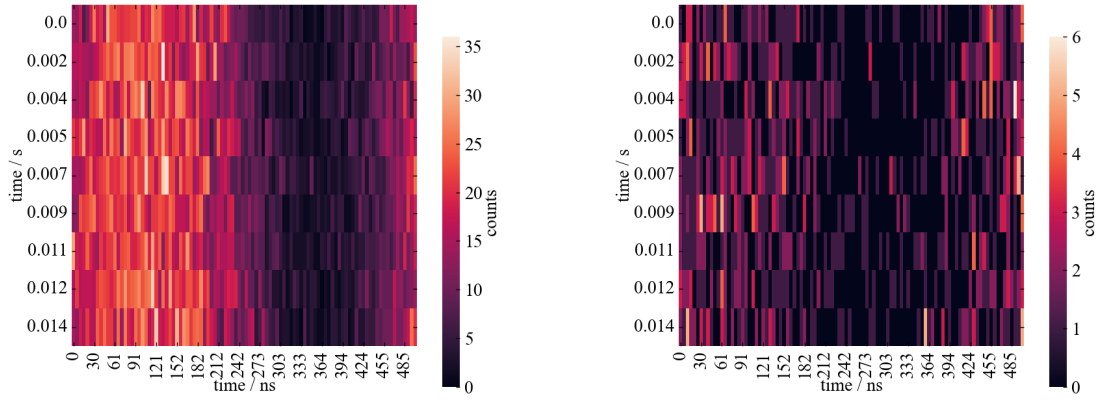

(a) Constant signal on SPCM

(b) Experiment pulsing of the signal on SPCM

Figure 3.17: Heat maps showing the phase drift over the bias stability time of 16 ms

In both figures 3.17(a) and 3.17(b), the beat signal is depicted inside the time interval given by the bias stability. Due to the low number of photons, which are detected when turning the signal on and off with

the experiment pulsing in 3.17(b), another heat map for a constant measured signal is shown in figure 3.17(a). In both figures, the phase is relatively stable, which confirms the bias stability calculated with the Allan deviation in section 3.4.

In this section, the assembly of a pulse generator as well as the method of turning the AOM on and off to simulate the pulse pattern used in the main experiment is described. It is possible to turn the AOM on and off without distorting the trigger signal so that the beat signal can still be reliably reconstructed. By folding the data, the form of the pulses in the signal can be retrieved. Furthermore, the phase shift can be visualized by entering the folded beat signal inside each measurement window into a heat map.

3.6 Conditional phase

The conditional phase shift is measured by comparing the events in both SPCMs, the one measuring the interference signal and the one measuring the reference signal, see figure 2.3. If two photons are measured inside a small time interval, called the coincidence interval, in both detectors, the events are entered in one histogram. In case a photon is registered only in the SPCM measuring the interference signal, the event is entered into a second histogram.

This sorting of the photons is shown in figure 3.18. Here the incident photons recorded by the time tagger are shown, as well as the defined time interval, which gives the condition in which histogram the photons are sorted. The coincidence interval is defined around the detection times of the photons from the interference signal. In the figure below, the photons from the interference signal are marked as blue bars and the photons from the reference signal are marked as purple bars. If two photons are detected in the light blue time interval, which is situated around the detection times of the photons from the interference signal (blue bar), then they are entered in the first histogram as described above. Otherwise they are entered in a second histogram.

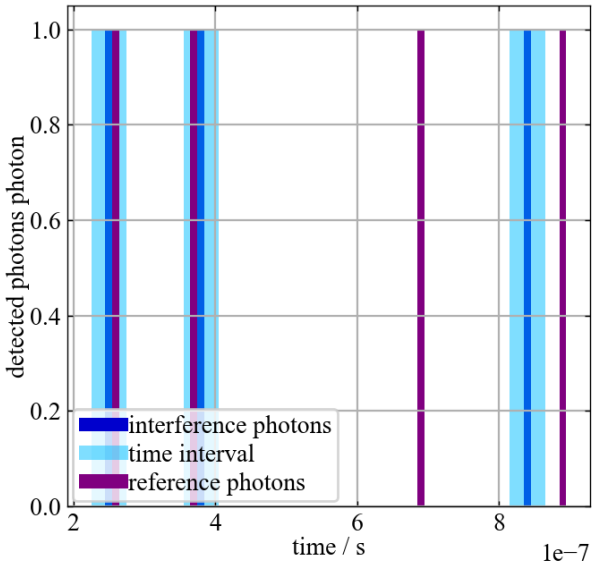

Figure 3.18: Conditional phase shift sketch

In the test setup discussed in this thesis, there are no phase shifting media introduced in the signal arm of the interferometer. Therefore, it is only shown, that the events on the SPCM behind the fiber coupler can be sorted according to their time of arrival compared to the time a photon arrives on the second SPCM. In an experimental setup, e.g. to measure the conditional phase shift introduced by a Rydberg blockade, the coincidence interval is approximately $T_{\text{coinc Ryd}} = (10 - 25)\text{ns}$[4] [19]. Since the coincidence interval is not defined by the main experiment conditions like e.g. the Rydberg blockade in highly excited atoms, it can be assigned an arbitrary value. For $T_{\text{coinc}} = 1\,\mu\text{s}$ the number of one and two photons being detected inside this time interval is similar. With the **FileWriter** data collection method it is possible to store the data such that the condition can be applied. Since no phase shifting medium is inserted into the interferometer and the conditional phase measurements are only a proof of the principle, the experiment is not pulsed. The AOMs are constantly turned on. The resulting histograms are shown in figure 3.19.

[4] from private conversation

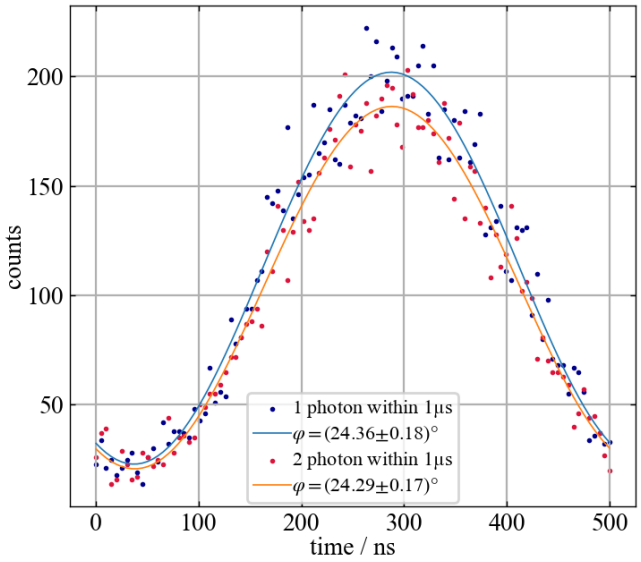

Figure 3.19: Conditional selection of photons in two histograms with coincidence interval $T_{\text{coinc}} = 1\,\mu\text{s}$

Both beat signals, the one extracted from two photons (orange plot) and one photon (blue plot) detected inside T_{coinc} are clearly visible. To these beat signals the function in equation 3.1 can be fitted. The phases resulting from the fits are listed in table 3.5.

	phase φ / °
1 photon in T_{coinc}	24.36 ± 0.18
2 photons in T_{coinc}	24.29 ± 0.17

Table 3.5: Fitted phases of conditionally selected photons

Both fitted phases overlap considering their uncertainties, which confirms the expected result since no phase shifting medium is inserted into the interferometer.

With the implemented interferometer it is possible to separate the incoming photons on the condition, that a second photon was measured in a fixed time interval close to the first in the two SPCM. In this setup no conditional phase shift was measured, which is to be expected, since there are no phase shifting media inserted into the signal beam of the interferometer.

CHAPTER 4

Conclusion & Outlook

Detection of conditional phase shifts is a way of characterizing quantum nonlinear media. The goal of this thesis was to build an interferometer which allows this detection. In this interferometer, the interference signal was created by a laser beam which was split in two beams. The frequency of each beam was shifted via acousto-optic modulators by respectively 80 MHz and 82 MHz resulting in a beat signal with a frequency of 2 MHz. The interferometer was adjusted and tested to introduce it into the Rubidium Rydberg Quantum Optics experiment in the Nonlinear Quantum Optics group in Bonn. To that end, the test setup was implemented with experiment-like distances and pulsed measurement of the interfering laser beams.

With this interferometer setup it was possible to reconstruct a clear beat signal for low laser intensities. By introducing a trigger signal to the setup, an automated and reliable method for the determination of the folding period for reconstructing the beat signal was found.

With a simulation of the raw photon data it was demonstrated that the unconditional phase could be retrieved with slightly different accuracies for different power ratios of the interfering beams. Furthermore it has shown, that the limiting factor while determining the phase for low photon numbers was the shot noise.

The stability of the phase of the interferometer in the time domain was characterized via the Allan deviation for two different lasers. The determined bias stability time $\tau_{\text{bias}} = 16\,\text{ms}$ for the distributed feedback (DFB) laser indicated that the phase is most stable over consecutive time intervals of the length τ_{bias} with a deviation of about 1°. An evaluation of the stability of the setup for the used extended cavity diode laser (ECDL) showed that it is less suited for the setup due to its higher noise, which could be visualized with the implemented Allan deviation. This difference in their stability curves resulted from the laser's different designs An evaluation of the phase stability of the interferometer shows that the noise of one of the used lasers, the ECDL, can be visualized and its frequency can be determined.

It was demonstrated that by using a pulse generator, it is possible to simulate the experimental sequence of pulsed measurement times and the beat signal can be retrieved despite the significant reduction of the raw data. Additionally, it was shown that the beat signal can be retrieved in the significantly smaller time interval of the bias stability.

A method to measure the conditional phase by defining a coincidence time was presented. In the

measurement of the conditional phase, there are no nonlinear media present introducing such a phase shift. Nonetheless, a sorting of the individual photons according to their relative incident times at the detectors was demonstrated.

Building on this thesis, the interferometer can be implemented and tested in a real experiment to measure the conditional phase shift. In this case, the interferometer has to be tested further to determine if and where there are other sources of disturbance.

In the test setup of the interferometer individual time tags were saved. In the current experiment, the time tags are saved in a histogram format. Therefore, implementing the interferometer into the experiment requires new software to be written to adapt to this change in recording the data.

If this interferometer is succesfully built into the experiment, it will be useful to make new obervations and demonstrate control over single photons [19].

Bibliography

[1] H. J. Kimble, *The quantum internet*, Nature **453** (2008), URL: https://www.nature.com/articles/nature07127 (cit. on p. 1).

[2] M. Benyoucef, *Photonic Quantum Technologies: Science and Applications*, Cambridge University Press, 2023 (cit. on p. 1).

[3] H. J. Kimble, *Optical π phase shift created with a single-photon pulse*, Nature **453** (2008), URL: https://www.science.org/doi/10.1126/sciadv.1600036 (cit. on p. 1).

[4] O. Firstenberg et al., *Measurement of Conditional Phase Shifts for Quantum Logic*, Physical Review Letters **75** (1995), URL: https://journals.aps.org/prl/abstract/10.1103/PhysRevLett.75.4710 (cit. on p. 1).

[5] O. Firstenberg et al., *Nonlinear Quantum Optics mediated by Rydberg Interactions*, J. Phys. B: at. Mol. Opt. Phys. **49** (2016), URL: https://journals.aps.org/prx/abstract/10.1103/PhysRevX.7.041010 (cit. on p. 1).

[6] T. Peyronel et al., *Quantum nonlinear optics with single photons enabled by strongly interacting atoms*, Nature **488** (2012), URL: https://www.nature.com/articles/nature11361 (cit. on p. 1).

[7] T. Peyronel et al., *Attractive photons in a quantum nonlinear medium*, Nature **502** (2013), URL: https://www.nature.com/articles/nature12512 (cit. on p. 1).

[8] T. Zahar, *Attractive photon interactions and bound states mediated by an ensemble of cold Rydberg atoms*, Master thesis: Weizmann Institute of Science, 2021 (cit. on pp. 1, 6, 18, 21).

[9] A. K. Speier, *Heterodyne interferometer for detection of conditional single-photon phase shifts*, Institut für Angewandte Physik, 2023 (cit. on p. 1).

[10] M. Fox, *Quantum Optics - An introduction*, Oxford master series in atomic, optical and laser physics, 2004, ISBN: 978–0–19–856672–4 (cit. on pp. 3, 4, 6).

[11] D. R. Paschotta, *Acousto-optic Modulators*, URL: https://www.rp-photonics.com/acousto_optic_modulators.html (cit. on p. 7).

[12] Swabian Instruments, *Time Tagger User Manual*, URL: https://www.swabianinstruments.com/static/documentation/TimeTagger/index.html (cit. on p. 9).

[13] P. Horowitz and W. Hill, *The Art of Electronics*, Cambridge University Press, 2015 (cit. on p. 21).

[14] D. W. Allan, *Statistics of Atomic Frequency Standards*, Proceedings of the IEEE (1966), URL: https://tf.nist.gov/general/pdf/7.pdf (cit. on p. 21).

[15] V. V. Vassiliev, S. A. Zibrov and V. L. Velichansky, *Compact extended-cavity diode laser for atomic spectroscopy and metrology*, 2006, URL: https://vitawave.ru/articles-p/eng/(2006)--RoSI--(Vas_Zib_Vel)--77_013102.pdf (cit. on p. 24).

[16] D. R. Paschotta, *Distributed Feedback Lasers*, URL: https://www.rp-photonics.com/distributed_feedback_lasers.html (cit. on p. 25).

[17] F. Engel, *Entwicklung eines FPGA basierten Pulsgenerators mit Nanosekunden-Auflösung für schnelle Rydberg-Experimente*, Bachelor thesis: 5. Physikalisches Institut Universität Stuttgart, 2013 (cit. on p. 27).

[18] A. Paris-Mandoki et al., *Free-Space Quantum Electrodynamics with a Single Rydberg Superatom*, Physical Review X (2017), URL: https://journals.aps.org/prx/abstract/10.1103/PhysRevX.7.041010 (cit. on p. 28).

[19] L. Drori et al., *Quantum vortices of strongly interacting photons*, Science **381** (2023), URL: https://www.science.org/doi/epdf/10.1126/science.adh5315 (cit. on pp. 32, 35).